

Dual-Modal Prototype Joint Learning for Compositional Zero-Shot Learning

Shiyu Zhang¹, Cheng Yan¹, Yang Liu², Chenchen Jing², Lei Zhou³, Wenjun Wang¹

¹Tianjin University, Tianjin, China

²Zhejiang University, Zhejiang, China

³Hainan University, Hainan, China

Abstract

Compositional Zero-Shot Learning (CZSL) aims to recognize novel compositions of attributes and objects by leveraging knowledge learned from seen compositions. Recent approaches have explored the use of Vision-Language Models (VLMs) to align textual and visual modalities. These methods typically employ prompt engineering, parameter-tuning, and modality fusion to generate rich textual prototypes that serve as class prototypes for CZSL. However, the modality gap results in textual prototypes being unable to fully capture the optimal representations of all class prototypes, particularly those with fine-grained features, which can be directly obtained from the visual modality. In this paper, we propose a novel Dual-Modal Prototype Joint Learning framework for the CZSL task. Our approach, based on VLMs, introduces prototypes in both the textual and visual modalities. The textual prototype is optimized to capture broad conceptual information, aiding the model’s generalization across unseen compositions. Meanwhile, the visual prototype is used to mitigate the classification errors caused by the modality gap and capture fine-grained details to distinguish images with similar appearances. To effectively optimize these prototypes, we design specialized decomposition modules and a joint learning strategy that enrich the features from both modalities. These prototypes not only capture key category information during training but also serve as crucial reference targets during inference. Experimental results demonstrate that our approach achieves state-of-the-art performance in the closed-world setting and competitive performance in the open-world setting across three publicly available CZSL benchmarks. These findings validate the effectiveness of our method in advancing compositional generalization.

1. Introduction

In human cognition, the ability to recombine existing concepts to form new ones is essential for quickly acquiring new knowledge, a skill known as compositional general-

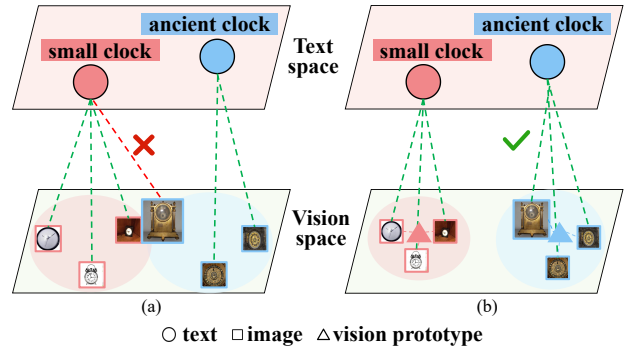


Figure 1. (a) Given an image of an ancient clock, which primarily carries the attribute "ancient" but also includes the semantic detail "small," the modality gap in VLM, diversity in image space, and fine-grained differences negatively affect the classification result. (b) To address this, we introduce prototypes in both modalities to improve modality alignment, facilitate fine-grained feature learning, and enable accurate classification during inference.

ization. Similarly, in computer vision, this ability is crucial for advancing models’ adaptability to novel situations, which has led to the development of Compositional Zero-Shot Learning (CZSL) [25, 30]. The goal of CZSL is to enable models to decompose and recombine concepts learned from seen compositions of attributes and objects, and then generalize to unseen compositions, thereby addressing the zero-shot image classification task. For instance, if a model is trained on compositions such as green clothes and red apples, it should be capable of recognizing novel compositions, like red clothes and green apples, during testing.

Thanks to the development of large pre-trained vision-language models such as CLIP [34], existing research has leveraged CLIP and employed approaches such as designing task-specific prompts [3, 20, 22, 29, 40, 41], decomposing composition text features [21], and developing modal fusion methods [8] to narrow the modality gap. These efforts improve the alignment between compositional labels and image features, enabling CLIP to perform effectively for CZSL.

However, several challenges and inherent problems in

the CZSL task still deserve attention. (1) Previous works have shown that the modality gap can be reduced but not completely eliminated [19]. This gap negatively impacts the CZSL task due to its current setup, where classification relies on the top-1 cross-modal retrieval result. As a consequence, the distance between true sample pairs from different modalities may be larger than that of false sample pairs, leading to errors caused by the modality gap, as shown in Fig. 1(a). (2) Existing methods primarily focus on inter-modal feature alignment and the use of various prompts [22, 29, 40] to enhance text features, yet they often overlook the importance of the visual modality. In CZSL tasks, where compositional text labels consist of multiple attributes and objects, the model must capture both the diversity and fine-grained details of categories. These features reside in the visual space, as each category contains multiple image instances, whereas only a single compositional text label is available. Therefore, relying solely on textual prototypes is insufficient to fully represent these visual features. For instance, as shown in Fig. 1(b), the image of an 'ancient clock' is very similar to that of a 'small clock,' and distinguishing between them is difficult without fine-grained visual information.

Based on the challenges and observations outlined above, we introduce a novel prototype-based joint learning framework called Dual-Modal Prototype Joint Learning (DPJL) for CZSL. Our approach utilizes prototypes from both modalities to capture key category information. The textual prototype adjusts the distribution of class centers in the text space and aligns with image features, enabling the model to learn class prototypes that represent broad concepts while exhibiting strong generalization. The visual prototype, on the other hand, refines the hypersphere boundaries of each class and captures fine-grained features that the textual prototype lacks by reducing intra-class distances and increasing inter-class distances in the image feature space. Additionally, we propose a dual-modal prototype joint learning strategy, where the two prototypes mutually reinforce each other to achieve optimal performance. Furthermore, as each composition consists of both attribute and object concepts, we design specific decomposition modules for these prototypes in both modalities to enhance their representational capacity. For testing, classification is not solely based on the top-1 cross-modal retrieval result but also considers the relationship with the corresponding visual prototype. In summary, our main contributions are as follows:

- We propose a novel prototype-based CZSL framework that leverages prototypes to enhance feature learning in both modalities and improve classification accuracy during inference. To the best of our knowledge, this is the first approach that utilizes dual-modal prototypes to enhance the generalization ability and fine-grained discrim-

inative power of the CZSL task.

- We design corresponding image feature decomposition modules for the prototypes of each modality and propose a joint learning strategy to optimize the prototypes, allowing them to mutually reinforce each other and achieve optimal performance.
- Experimental results on three publicly available CZSL datasets demonstrate that our method achieves state-of-the-art performance in the closed-world setting and outperforms competing methods by a significant margin on 2 out of 3 datasets in the open-world setting.

2. Related Work

Compositional Zero-Shot Learning. Previous methods for CZSL can be grouped into two strategies: (1) Uniform features representation learning, which establish relationships between compositions and primitives such as attributes and objects, then embed both images and compositions into a shared space, using a single classifier to directly predict unseen compositions [1, 16, 24, 25, 27, 31]. (2) Multi-branch feature learning, which designs parallel discriminative modules for attributes, objects, and compositions while considering the importance of visual feature discriminability [13, 15, 18, 28, 36, 38]. Recently, benefiting from the development of pre-trained Vision-Language Models (VLMs) and their strong generalization capabilities, researchers have increasingly applied VLM to CZSL [12, 21, 22, 29, 40]. For example, Nayak et al. [29] applied a method that uses soft prompts, treating the attributes and objects defining classes as learnable tokens. Xu et al. [41] constructed a graph [39] of object-attribute compositions, feeding the updated composition representations into soft prompts. Lu et al. [21] decomposed states and objects in language features and further integrated them with image features. Huang et al. [8] established three recognition branches to jointly model attributes, objects, and compositions, aligning branch-specific prompt representations with decomposed visual features. Li et al. [17] proposed a context-based, diversity-driven specificity learning framework, considering the varying levels of specificity in attributes. Our model is built on the VLM, with specific modules such as modality prototypes and decomposition modules designed to improve modality alignment and promote fine-grained feature learning.

Prototype Learning. The prototype network aims to learn a metric space for classification by computing distances to the prototype representations of each class [37]. It has demonstrated advantages in open-set recognition and few-shot tasks [6, 43]. Recently, some studies have introduced prototypes into CZSL [16, 35], where they obtain the prototypes by averaging image features, with the prototypes derived from a single modality. Our work differs from the aforementioned prototype-updating methods. We introduce

textual and visual prototypes during the training phase and make them both learnable. By aligning the dual-modal prototypes with image features, we learn textual prototypes that represent broad concepts and visual prototypes that capture fine-grained features.

3. Method

Overview. The CZSL task requires the model to generalize well to unseen compositions while also discriminating fine-grained differences among similar compositions. To address this challenge, we propose a novel framework called Dual-Modal Prototype Joint Learning (DPJL) for CZSL, which establishes a new paradigm of joint learning and inference of textual prototypes and visual prototypes. As illustrated in Fig. 2, the input image is passed through the image encoder, and the extracted global features are simultaneously fed into both the textual prototype learning module and the visual prototype learning module, each with three distinct pipelines: attribute, object, and composition. The learnable visual prototypes are optimized based on visual features and a decomposition module implemented using an MLP. The textual prototypes are derived from learnable prompts and are optimized using both text and image features, which are decoupled through a cross-attention-based decomposition module. To enhance inter-modal learning, a dual-prototype joint training strategy is proposed, enriching both the visual and textual prototypes. During inference, the final probability score is obtained by summing the probabilities from both prototypes.

3.1. Problem Formulation

In CZSL, compositional labels consist of attributes and objects. Attributes are denoted as $a \in \mathcal{A}$, objects as $o \in \mathcal{O}$, and compositions as $y \in \mathcal{Y}$, where $\mathcal{Y} = \mathcal{A} \times \mathcal{O}$. The compositional label space is divided into seen compositions \mathcal{Y}_s and unseen compositions \mathcal{Y}_u , with $\mathcal{Y}_s \cap \mathcal{Y}_u = \emptyset$. The training set is defined as $\mathcal{T} = (x, y), |, x \in \mathcal{X}, y \in \mathcal{Y}_s$, where \mathcal{X} represents the image space. During testing, the model must classify images from both seen and unseen compositions. CZSL can be categorized into closed-world and open-world settings based on the treatment of unseen compositions [23]. In the closed-world setting, unseen compositions \mathcal{Y}_u are provided as prior knowledge, and the prediction space is $\mathcal{Y}_{pred} = \mathcal{Y}_s \cup \mathcal{Y}_u$. In contrast, in the open-world setting, unseen compositions include all possible attribute-object compositions, and the prediction space is $\mathcal{Y}_{pred} = \mathcal{A} \times \mathcal{O}$.

3.2. Visual Representation

Following prior research [8], we use an image encoder to extract visual features. All parameters of the encoder are frozen, and an adapter [5] is incorporated to allow fine-tuning by updating only a minimal set of parameters, thereby enhancing feature learning. Specifically, given an

image x , the global image feature $f_v^{cls} = E_v(x)$ is extracted using the image encoder E_v .

3.3. Textual Prototype Learning

The textual prototypes are designed to capture class-specific text representations. To ensure the model generalizes well to unseen compositions, as proposed in [8], we implement three recognition branches to learn distinct text prototypes corresponding to attributes, objects, and compositions. Furthermore, we design a decomposition module to decouple the visual features into attribute-based and object-based components, improving alignment within our multi-branch structure.

Text Representation. Following [8, 29, 40], we utilize the text encoder from the CLIP [34] model and keep it frozen. First, we construct the attribute prompt $\theta_i^a = [p_0^a, \dots, p_m^a, w_i^a]$, the object prompt $\theta_j^o = [p_0^o, \dots, p_m^o, w_j^o]$, and the composition prompt $\theta_{i,j}^c = [p_0^c, \dots, p_m^c, w_i^a, w_j^o]$. These prompts are treated as learnable parameters and fed into the text encoder E_t , producing the attribute text feature $t_i^a = E_t(\theta_i^a)$, the object text feature $t_j^o = E_t(\theta_j^o)$, and the composition text feature $t_{i,j}^c = E_t(\theta_{i,j}^c)$. The text representations are treated as textual prototypes, denoted as follows:

$$t^a = [t_1^a, t_2^a, \dots, t_{|\mathcal{A}|}^a], \quad t^o = [t_1^o, t_2^o, \dots, t_{|\mathcal{O}|}^o], \quad (1)$$

$$t^c = [t_{1,1}^c, t_{1,2}^c, \dots, t_{1,j}^c, \dots, t_{|\mathcal{Y}_s|}^c], \quad (2)$$

where $|\mathcal{A}|$ and $|\mathcal{O}|$ denote the number of attributes and objects, respectively, $|\mathcal{Y}_s|$ indicates the number of seen compositions during the training phase.

Cross-Attention Decomposition Module. To learn optimal textual prototypes for each branch, aligning them with the corresponding visual representations is crucial due to the modality gap. Therefore, we propose a cross-attention-based image feature decomposition module to bridge this gap. Specifically, we use the original image feature f_v^{cls} as the composition visual representation f^c , which is then employed to optimize the composition textual prototype. For the attribute and object branches, we utilize a Cross-Attention (CA) module [4] to transfer the composition feature into attribute-specific and object-specific features. The cross-attention and multi-head mechanisms of the CA module provide an effective transformation of visual features based on the textual descriptions of attributes or objects, which helps reduce the modality gap. We denote the Attribute Decomposition Cross-Attention model as **AD-CA** and the Object Decomposition Cross-Attention model as **OD-CA**. The query, key, and value are derived as follows:

$$q = f^c W_i^q, \quad k = t W_i^k, \quad v = t W_i^v, \quad (3)$$

where W_i^q , W_i^k , and $W_i^v \in \mathbb{R}^{d \times d_k}$ are the parameter matrices, with $d_k = d/h$, where h is the number of attention

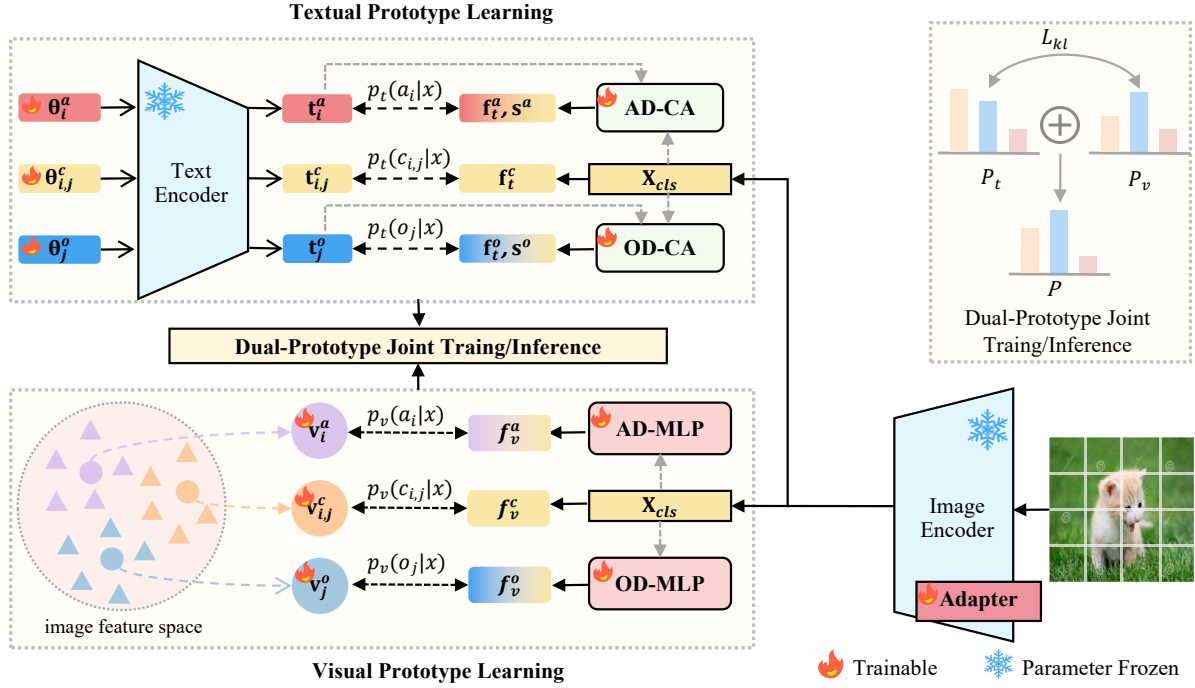


Figure 2. The proposed DPJL framework primarily consists of textual and visual prototype learning components, each featuring three distinct pipelines: attribute, object, and composition, all aimed at feature and prototype learning. For intra-modal learning, a dedicated decomposition module is designed to improve the feature quality. For inter-modal learning, a dual-prototype joint training strategy is introduced, enabling the optimization of both textual and visual prototypes. During inference, the final probability score is obtained by summing the probabilities of the two prototypes.

heads. The attention weights and output for each head are:

$$\text{Score}_i = \text{softmax} \left(\frac{qk^T}{\sqrt{d_k}} \right), \quad o_i = \text{softmax} \left(\frac{qk^T}{\sqrt{d_k}} \right) v, \quad (4)$$

where $i = 1, 2, \dots, h$. The multi-head output is obtained by concatenating and linearly projecting:

$$o = \text{Concat}(o_1, o_2, \dots, o_h) W_o, \quad (5)$$

The final attention score is averaged, and the output o is then passed through a feed-forward network, layer normalization, and a residual connection:

$$\text{Score} = \frac{1}{h} \sum_{i=1}^h \text{Score}_i, \quad \tilde{o} = f^c + \text{FFN}(\text{LN}(f^c + o)), \quad (6)$$

where $W_o \in \mathbb{R}^{d \times d}$ is the weight matrix.

Finally, the compositional visual representations are fed into the **AD-CA** module to extract the attribute visual representations, f_t^a , along with the corresponding attention weights, s^a . Likewise, the object image features, f_t^o , and attention weights, s^o , are obtained through the **OD-CA** module.

Textual Prototype Training. Given the textual prototypes and the decomposed image features for each branch, we

compute the probabilities for attributes, objects, and their compositions. Unlike previous studies [8, 17], which typically treated attributes and objects independently, our approach takes into account their interdependence in CZSL. Therefore, while calculating the probability scores for attributes and objects using the decomposed image features and their corresponding textual prototypes, we also integrate the attention weights between the original image features and the textual prototypes. This integration enhances the accuracy of predictions for attributes and objects. The specific calculations for these probabilities are as follows:

$$p_t(a_i|x) = \frac{\exp((f_t^a \cdot t_i^a + s_i^a)/\tau)}{\sum_{k=1}^{|A|} \exp((f_t^a \cdot t_k^a + s_k^a)/\tau)}, \quad (7)$$

$$p_t(o_j|x) = \frac{\exp((f_t^o \cdot t_j^o + s_j^o)/\tau)}{\sum_{k=1}^{|O|} \exp((f_t^o \cdot t_k^o + s_k^o)/\tau)}, \quad (8)$$

$$p_t(c_{i,j}|x) = \frac{\exp(f^c \cdot t_{i,j}^c/\tau)}{\sum_{k=1}^{|Y_s|} \exp(f^c \cdot t_k^c/\tau)} \quad (9)$$

where $\tau \in \mathbb{R}$ denotes the temperature parameter, which is pre-trained in CLIP. Subsequently, we compute the cross-entropy loss for each branch as follows:

$$\mathcal{L}_t^a = -\frac{1}{|\mathcal{X}|} \sum_{x \in \mathcal{X}} \log p_t(a|x), \quad (10)$$

$$\mathcal{L}_t^o = -\frac{1}{|\mathcal{X}|} \sum_{x \in \mathcal{X}} \log p_t(o|x), \quad (11)$$

$$\mathcal{L}_t^c = -\frac{1}{|\mathcal{X}|} \sum_{x \in \mathcal{X}} \log p_t(c|x), \quad (12)$$

Therefore, the total loss for the textual prototypes learning module \mathcal{L}_t is defined as:

$$\mathcal{L}_t = \mathcal{L}_t^a + \mathcal{L}_t^o + \mathcal{L}_t^c \quad (13)$$

3.4. Visual Prototype Learning

The textual prototype learning module described above is designed to narrow the gap between the visual and textual modalities, facilitating the learning of a unified class prototype. Previous studies [32] have demonstrated that the class prototype exists in the overlapping region between the visual and text spaces. As shown in Fig. 3 (a), \mathbf{z}_j is the class prototype of CLIP, which can be presented by two features from both modalities:

$$\mathbf{z}_j = \sqrt{a}\mathbf{z}_j^x + \sqrt{1-a}\mathbf{z}_j^t, \quad (14)$$

where \mathbf{z}_j^x is derived from the vision space and \mathbf{z}_j^t shows the component from the orthogonal subspace such that $\mathbf{z}_j^{x\top} \mathbf{z}_j^t = 0$, containing information unique to the textual modality. The class prototype \mathbf{z}_j in the intersection area embodies shared information from both modalities. However, due to the gap between these modalities, the class prototype in the overlapping region is still influenced by this discrepancy, which means the ideal state of Fig. 3(b) is almost impossible to reach. Given that the core of the CZSL task is image classification, the optimal solution for all class prototypes must lie within the vision space. Thus the balance of learning should be appropriately tilted toward visual modality. To this end, we introduce visual prototype learning.

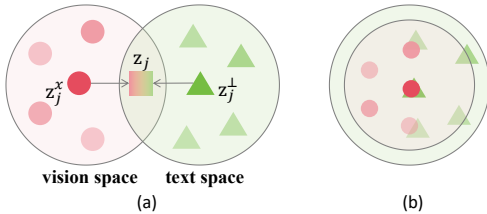


Figure 3. (a) Illustration of the visual and text spaces, where the class prototype \mathbf{z}_j resides in the overlapping region. (b) Ideal scenario where the visual space is fully covered by the text space.

Visual Prototype Construction. We denote the attribute visual prototypes as v^a and the object visual prototypes as v^o , as follows:

$$v^a = [v_1^a, v_2^a, \dots, v_{|\mathcal{A}|}^a], \quad v_i^a \in \mathbb{R}^{1 \times d} \quad (15)$$

$$v^o = [v_1^o, v_2^o, \dots, v_{|\mathcal{O}|}^o], \quad v_j^o \in \mathbb{R}^{1 \times d} \quad (16)$$

where $|\mathcal{A}|$ and $|\mathcal{O}|$ represent the number of attributes and objects, and d represents the dimension of image features.

Given the significant variability in image features representing the same attribute across different objects in CZSL, using the average image features from samples within the same category to define visual prototypes, as proposed by [37], has certain limitations. However, a key advantage is that other modalities, such as the text modality, have successfully learned robust class prototypes. Therefore, we utilize the textual feature from a pre-trained language model (PLM) [14, 33, 34] as the initial visual prototypes:

$$v_i^a = E_l(w_i^a), \quad v_j^o = E_l(w_j^o), \quad (17)$$

where E_l represents the text encoder derived from the PLM. Given that CZSL requires the classification of unseen compositions during testing, we set the attribute visual prototypes, v^a , and the object visual prototypes, v^o , as learnable parameters, and concatenate them to obtain the composition visual prototype, v^c :

$$v_{i,j}^c = E_c([v_i^a, v_j^o]), \quad (18)$$

where E_c is a fully connected layer that projects the concatenated composition visual prototype into the visual embedding space, ensuring consistency with the dimensionality of the image features.

MLP Decomposition Module. To decompose features in the visual modality for visual prototype learning, we design an MLP-based image feature decomposition module. We replace the CA with an MLP because it is an intra-modality learning process. Therefore, the visual features can be directly projected for decomposition. Specifically, for the composition branch, we directly use the global image feature f_v^{cls} as the composition image feature f^c . For the attribute and object branches, the decomposed image features are derived by transforming the composition image feature f^c through two MLP modules, **AD-MLP** for attributes and **OD-MLP** for objects, denoted as:

$$f_v^a = MLP(f^c), \quad f_v^o = MLP(f^c), \quad f_v^c = f^c \quad (19)$$

Visual Prototype Training. We cluster image features of the same category to form visual prototypes by calculating the cosine similarity between the image features and the visual prototypes. The specific probability calculations for each branch are outlined as follows:

$$p_v(a_i|x) = \frac{\exp(f^c \cdot v_i^a/\tau)}{\sum_{k=1}^{|\mathcal{A}|} \exp(f^c \cdot v_k^a/\tau)}, \quad (20)$$

$$p_v(o_j|x) = \frac{\exp(f^c \cdot v_j^o/\tau)}{\sum_{k=1}^{|\mathcal{O}|} \exp(f^c \cdot v_k^o/\tau)}, \quad (21)$$

$$p_v(c_{i,j}|x) = \frac{\exp(f^c \cdot v_{i,j}^c/\tau)}{\sum_{k=1}^{|\mathcal{Y}_s|} \exp(f^c \cdot v_k^c/\tau)} \quad (22)$$

Subsequently, we calculate the cross-entropy loss for each branch:

$$\mathcal{L}_v^a = -\frac{1}{|\mathcal{X}|} \sum_{x \in \mathcal{X}} \log p_v(a|x), \quad (23)$$

$$\mathcal{L}_v^o = -\frac{1}{|\mathcal{X}|} \sum_{x \in \mathcal{X}} \log p_v(o|x), \quad (24)$$

$$\mathcal{L}_v^c = -\frac{1}{|\mathcal{X}|} \sum_{x \in \mathcal{X}} \log p_v(c|x), \quad (25)$$

Therefore, the total loss for the visual prototypes learning module \mathcal{L}_v is defined as:

$$\mathcal{L}_v = \mathcal{L}_v^a + \mathcal{L}_v^o + \mathcal{L}_v^c \quad (26)$$

3.5. Dual-Prototype Joint Training and Inference

Training. To jointly learn optimal textual and visual prototypes, we use Kullback-Leibler (KL) divergence to align the distributions of the dual-modal prototypes. Since the textual prototypes are relatively well-established, while the visual prototypes are trained from scratch and may be prone to biases, we designate the textual prototypes as the target distribution and the visual prototypes as the approximate distribution. The loss function is:

$$\mathcal{L}_{kl} = D_{KL}(P_t \| P_v) = \sum_x P_t(x) \log \frac{P_t(x)}{P_v(x)} \quad (27)$$

where P_t represents the probability distribution estimated by the textual prototypes, while P_v represents the probability distribution estimated by the visual prototypes. Consequently, the total loss for the joint learning of the dual-modal prototypes, denoted as \mathcal{L} , is expressed as follows:

$$\mathcal{L} = \mathcal{L}_t + \mathcal{L}_v + \mathcal{L}_{kl} \quad (28)$$

By minimizing the loss function, we can obtain the optimal textual prototypes and visual prototypes:

$$\mathbf{t}^*, \mathbf{v}^* = \arg \min_{\mathbf{t}, \mathbf{v}} (\mathcal{L}) \quad (29)$$

Inference. After obtaining the optimal textual and visual prototypes, we combine them for classification. Specifically, during inference, we compute the sum of the probabilities from both prototypes for each branch, which serves as the final probability for that branch:

$$p(a_i|x) = \alpha p_t(a_i|x) + (1 - \alpha) p_v(a_i|x), \quad (30)$$

$$p(o_j|x) = \alpha p_t(o_j|x) + (1 - \alpha) p_v(o_j|x), \quad (31)$$

$$p(c_{i,j}|x) = \alpha p_t(c_{i,j}|x) + (1 - \alpha) p_v(c_{i,j}|x), \quad (32)$$

where α represents the weighting coefficient used to balance the influence of the different prototypes. The probability of the final prediction for a given sample is calculated

as the sum of the composition probability, object probability, and attribute probability:

$$p'(c_{i,j}|x) = p(c_{i,j}|x) + p(a_i|x) + p(o_j|x). \quad (33)$$

The final predicted composition is:

$$y' = \arg \max_{c_{i,j} \in \mathcal{Y}^{pred}} (p'(c_{i,j}|x)) \quad (34)$$

4. Experiments

4.1. Experiments Setting

Datasets. We evaluated the model’s performance on three datasets: UT-Zappos [42], MIT-States [10], and C-GQA [26]. UT-Zappos is a large shoe dataset consisting of 16 attributes and 12 objects. MIT-States is a diverse collection of everyday objects, featuring 115 attributes and 245 objects. C-GQA is the largest dataset for the CZSL task, derived from the GQA dataset [9], containing 453 attributes and 870 objects. We followed the dataset split standards from previous studies [27, 29] and the statistics are provided in Tab. 1.

Table 1. The statistics of three CZSL datasets.

Dataset			Train		Val			Test		
	\mathcal{A}	\mathcal{O}	\mathcal{Y}_s	\mathcal{X}	\mathcal{Y}_s	\mathcal{Y}_u	\mathcal{X}	\mathcal{Y}_s	\mathcal{Y}_u	\mathcal{X}
MIT-States	115	245	1.2k	30k	300	300	10k	400	400	13k
UT-Zappos	16	12	83	23k	15	15	3k	18	18	3k
C-GQA	413	674	5.5k	27k	1.2k	1k	7k	888	923	5k

Metrics. To comprehensively evaluate the model’s performance, similar to [8, 17], we follow the open-world and closed-world setting and use the following four evaluation metrics: (1) Accuracy on seen compositions (S): the accuracy of the best visible pair combinations. (2) Accuracy on unseen compositions (U): the accuracy of the best invisible pair combinations. (3) Harmonic mean (HM): the harmonic mean of the accuracy on seen and unseen compositions. (4) Area Under the Curve (AUC).

Implementation Details. To ensure fairness, we adopt the parameter settings established by previous research, utilizing the pre-trained CLIP ViT-L model [34] as our image/text encoder. The visual prototypes are initialized by the text embedding from the CLIP. During training, we use the Adam optimizer in conjunction with a StepLR learning rate scheduler, where the learning rate decays by a factor of 0.5 every 3 epochs. For the UT-Zappos and MIT-States datasets, the learning rate is 5×10^{-4} and weight decay is 1×10^{-5} ; for the C-GQA dataset, the learning rate is 5×10^{-5} with the same weight decay. Training is conducted for 20 epochs in total, and during the testing phase, the default setting for the hyperparameter α is 0.5. All training and testing are conducted on NVIDIA A6000 GPUs.

Table 2. The experimental results for both closed/open-world settings. The best performance are highlighted in bold.

Method	Venue	C-GQA				UT-Zappos				MIT-States			
		S	U	HM	AUC	S	U	HM	AUC	S	U	HM	AUC
Closed-world Results													
CLIP[34]	ICML'21	7.5	25.0	8.6	1.4	15.8	49.1	15.6	5.0	30.2	46.0	26.1	11.0
CoOp[44]	IJCV'22	20.5	26.8	17.1	4.4	52.1	49.3	34.6	18.8	34.4	47.6	29.8	13.5
CSP[29]	ICLR'23	28.8	26.8	20.5	6.2	64.2	66.2	46.6	33.0	46.6	49.9	36.3	19.4
DFSP(i2t)[21]	CVPR'23	35.6	29.3	24.3	8.7	64.2	66.4	45.1	32.1	47.4	52.4	37.2	20.7
DFSP(BiF)[21]	CVPR'23	36.5	32.0	26.2	9.9	63.3	69.2	47.1	33.5	47.1	52.8	37.7	20.8
DFSP(t2i)[21]	CVPR'23	38.2	32.0	27.1	10.5	66.7	71.7	47.2	36.0	46.9	52.0	37.3	20.6
DLM[7]	AAAI'24	32.4	28.5	21.9	7.3	67.1	72.5	52.0	39.6	46.3	49.8	37.4	20.0
ProLT[11]	AAAI'24	39.5	32.9	27.7	11.0	66.0	70.1	49.4	36.1	49.1	51.0	38.2	21.1
PLID[3]	ECCV'24	38.8	33.0	27.9	11.0	67.3	68.8	52.4	38.7	49.7	52.4	39.0	22.1
CDS-CZSL[17]	CVPR'24	38.3	34.2	28.1	11.1	63.9	74.8	52.7	39.5	50.3	52.9	39.2	22.4
Troika[8]	CVPR'24	41.0	35.7	29.4	12.4	66.8	73.8	54.6	41.7	49.0	53.0	39.3	22.1
DPJL(Ours)		46.0	40.2	34.9	16.3	71.9	76.3	58.5	47.9	51.8	52.6	40.4	23.3
Open-world Results													
CLIP[34]	ICML'21	7.5	4.6	4.0	0.3	15.7	20.6	11.2	2.2	30.1	14.3	12.8	3.0
CoOp[44]	IJCV'22	21.0	4.6	5.5	0.7	52.1	31.5	28.9	13.2	34.6	9.3	12.3	2.8
CSP[29]	ICLR'23	28.7	5.2	6.9	1.2	64.1	44.1	38.9	22.7	46.3	15.7	17.4	5.7
DFSP(i2t)[21]	CVPR'23	35.6	5.6	9.0	1.9	64.3	53.8	41.2	26.4	47.2	18.2	19.1	6.7
DFSP(BiF)[21]	CVPR'23	36.5	7.6	10.6	2.4	63.5	57.2	42.7	27.6	47.1	18.1	19.2	6.7
DFSP(t2i)[21]	CVPR'23	38.2	7.2	10.4	2.4	66.8	60.0	44.0	30.3	47.5	18.5	19.3	6.8
PLID[3]	ECCV'24	39.1	7.5	10.6	2.5	67.6	55.5	46.6	30.8	49.1	18.7	20.4	7.3
CDS-CZSL[17]	CVPR'24	37.6	8.2	11.6	2.7	64.7	61.3	48.2	32.3	49.4	21.8	22.1	8.5
Troika[8]	CVPR'24	40.8	7.9	10.9	2.7	66.4	61.2	47.8	33.0	48.8	18.4	20.1	7.2
DPJL(Ours)		46.0	11.5	15.5	4.6	71.9	66.6	54.5	41.4	51.8	19.9	22.0	8.3

4.2. Main Results

We comprehensively evaluate our model under both closed-world and open-world settings, comparing it with recent CLIP-based CZSL methods from the past two years, including: CLIP[34], CoOp[44], CSP[29], DFSP[21], DLM[7], ProLT[11], PLID[3], CDS-CZSL[17], and Troika[8]. The results are presented in Tab. 2. In the closed-world setting, our DPJL achieves SOTA performance across all three datasets on nearly all metrics. Specifically, DPJL improves the HM by +5.5%, +3.9%, and +1.1%, and the AUC by +3.9%, +6.2%, and +1.2%, respectively, across the three datasets, demonstrating the effectiveness of the proposed method. In the open-world setting, DPJL significantly outperforms competing methods on the UT-Zappos and C-GQA datasets, with HM improvements of +6.7% and +4.6%, and AUC improvements of +8.4% and +1.9%, respectively.

For the MIT-States dataset, which contains substantial label noise [2], there are instances where a single image satisfies multiple compositional pairs with hierarchical relationships. This issue is particularly pronounced in open-world settings. CDS-CZSL[17] incorporates a specialized module that prioritizes more distinct attributes, which helps reduce the compositional space in open-world scenarios, especially on the MIT-States dataset. Consequently, CDS-

CZSL achieves slightly better performance than our method on MIT-States, but its effectiveness is not as pronounced on the other two datasets. In contrast, our model demonstrates greater generalizability, as DPJL significantly outperforms all competing methods on two other challenging datasets, particularly on C-GQA, which involves complex backgrounds and multiple objects.

4.3. Ablation Study

Ablation study on prototypes. To demonstrate the effectiveness of prototype-based learning, we conduct ablation experiments under a closed-world setting on the UT-Zappos and MIT-States datasets. We sequentially remove the textual and visual prototypes during both training and inference, as well as inference only. From the results in both the 'Training and Inference' and 'Inference' panels, we observe that removing either the textual or visual prototypes leads to a significant performance decrease, highlighting the importance of dual-modal prototype. Notably, we remove only one prototype during the testing phase, while retaining all prototypes during training. Although this approach results in some performance decline, the decrease is less pronounced than if a prototype were removed during training. This finding suggests that our dual-modal prototype joint learning strategy enables the textual and visual prototypes



Figure 4. Qualitative results. The term ‘w/o vp’ refers to the text-prototype-based method, while the green font indicates correct labels and the red font indicates incorrect labels.

to mutually enhance each other’s learning.

Table 3. Results of ablation experiments on prototypes. ‘tp’/‘vp’ represents the text/visual prototypes.

		UT-Zappos				MIT-States			
<i>tp</i>	<i>vp</i>	S	U	HM	AUC	S	U	HM	AUC
Training and inference									
✓	✓	71.9	76.3	58.5	47.9	51.8	52.6	40.4	23.3
✓	✗	64.4	70.7	51.9	37.8	47.1	52.1	37.8	20.8
✗	✓	65.8	72.3	55.3	42.1	50.5	49.4	37.6	20.7
Inference									
✓	✓	71.9	76.3	58.5	47.9	51.8	52.6	40.4	23.3
✓	✗	69.2	75.1	56.7	44.2	51.3	52.3	40.4	23.0
✗	✓	69.5	76.4	57.8	46.4	48.7	50.6	37.3	20.4

Ablation study on decomposition modules. We exchange the decomposition modules on both prototype learning components to evaluate their capacity to the overall performance. As shown in Tab. 4, the CA-/MLP-based decomposition module achieves the best effect for textual/visual prototype learning respectively. The results confirm that it is more effective to achieve modality alignment after feature fusion, while an MLP-based transformation can be directly applied within the same modality.

Table 4. Results of ablation experiments on the decomposition modules. i2t/i2v represents the image feature decoupling method used in text/visual prototype learning, respectively.

		UT-Zappos				MIT-States			
i2t	i2v	S	U	HM	AUC	S	U	HM	AUC
CA	MLP	71.9	76.3	58.5	47.9	51.8	52.6	40.4	23.3
CA	CA	67.1	75.2	54.7	42.0	50.9	51.6	39.6	22.3
MLP	CA	67.3	76.2	55.7	44.2	50.8	52.5	39.6	22.8
MLP	MLP	69.5	73.1	58.5	45.3	50.0	51.4	38.8	21.8

4.4. Qualitative Results

We visualize the qualitative results of the model on the C-GQA and MIT-States datasets in Fig. 4. Specifically, we present both successful and failure cases of the proposed DPJL model, as well as those from the text-prototype-based method, denoted as ‘w/o vp’. From the results, it is evident that DPJL can accurately distinguish between similar compositions, such as ‘‘large painting’’ and ‘‘large picture,’’ or ‘‘broken bottle’’ and ‘‘spilled bottle,’’ whereas the method based solely on text prototypes struggles to distinguish between compositions with similar visual appearances. This indicates that DPJL has successfully learned fine-grained features of compositions. In failure cases, although the model does not always correctly identify the composition, it often manages to classify one of the primitives correctly. Upon inspecting the misclassified compositions, we notice that they are typically semantically similar to the true labels or involve some degree of ambiguity.

5. Conclusion

In this paper, we propose a novel method for the CZSL task. Recognizing the inherent advantages of the visual modality in CZSL, we introduce visual prototypes to enhance the model’s ability to capture fine-grained information in the visual space. We also develop tailored decomposition modules and a joint learning strategy to enhance feature representation, allowing the model to optimize prototypes across both modalities for the first time. These prototypes capture essential category information during training and act as crucial reference points during inference. Our experimental results demonstrate state-of-the-art performance in the closed-world setting and competitive results in the open-world setting across three public CZSL datasets, showcasing the effectiveness of our proposed method.

References

- [1] Muhammad Umer Anwaar, Zhihui Pan, and Martin Kleinsteuber. On leveraging variational graph embeddings for open world compositional zero-shot learning. In *Proceedings of the 30th ACM International Conference on Multimedia*, pages 4645–4654, 2022. 2
- [2] Yuval Atzmon, Felix Kreuk, Uri Shalit, and Gal Chechik. A causal view of compositional zero-shot recognition. *Advances in Neural Information Processing Systems*, 33:1462–1473, 2020. 7
- [3] Wentao Bao, Lichang Chen, Heng Huang, and Yu Kong. Prompting language-informed distribution for compositional zero-shot learning. In *Proceedings of the European Conference on Computer Vision (ECCV)*, 2024. 1, 7
- [4] Chun-Fu Richard Chen, Quanfu Fan, and Rameswar Panda. Crossvit: Cross-attention multi-scale vision transformer for image classification. In *Proceedings of the IEEE/CVF international conference on computer vision*, pages 357–366, 2021. 3
- [5] Shoufa Chen, Chongjian Ge, Zhan Tong, Jiangliu Wang, Yibing Song, Jue Wang, and Ping Luo. Adaptformer: Adapting vision transformers for scalable visual recognition. *Advances in Neural Information Processing Systems*, 35:16664–16678, 2022. 3
- [6] Jianlong Fu, Heliang Zheng, and Tao Mei. Look closer to see better: Recurrent attention convolutional neural network for fine-grained image recognition. In *Proceedings of the IEEE conference on computer vision and pattern recognition*, pages 4438–4446, 2017. 2
- [7] Xiaoming Hu and Zilei Wang. A dynamic learning method towards realistic compositional zero-shot learning. In *Proceedings of the AAAI Conference on Artificial Intelligence*, pages 2265–2273, 2024. 7
- [8] Siteng Huang, Biao Gong, Yutong Feng, Min Zhang, Yiliang Lv, and Donglin Wang. Troika: Multi-path cross-modal traction for compositional zero-shot learning. In *Proceedings of the IEEE/CVF Conference on Computer Vision and Pattern Recognition*, pages 24005–24014, 2024. 1, 2, 3, 4, 6, 7
- [9] Drew A Hudson and Christopher D Manning. Gqa: A new dataset for real-world visual reasoning and compositional question answering. In *Proceedings of the IEEE/CVF conference on computer vision and pattern recognition*, pages 6700–6709, 2019. 6
- [10] Phillip Isola, Joseph J Lim, and Edward H Adelson. Discovering states and transformations in image collections. In *Proceedings of the IEEE conference on computer vision and pattern recognition*, pages 1383–1391, 2015. 6
- [11] Chenyi Jiang and Haofeng Zhang. Revealing the proximate long-tail distribution in compositional zero-shot learning. In *Proceedings of the AAAI Conference on Artificial Intelligence*, pages 2498–2506, 2024. 7
- [12] Chenchen Jing, Yukun Li, Hao Chen, and Chunhua Shen. Retrieval-augmented primitive representations for compositional zero-shot learning. In *Proceedings of the AAAI Conference on Artificial Intelligence*, pages 2652–2660, 2024. 2
- [13] Shyamgopal Karthik, Massimiliano Mancini, and Zeynep Akata. Kg-sp: Knowledge guided simple primitives for open world compositional zero-shot learning. In *Proceedings of the IEEE/CVF Conference on Computer Vision and Pattern Recognition*, pages 9336–9345, 2022. 2
- [14] Jacob Devlin Ming-Wei Chang Kenton and Lee Kristina Toutanova. Bert: Pre-training of deep bidirectional transformers for language understanding. In *Proceedings of naacL-HLT*, page 2. Minneapolis, Minnesota, 2019. 5
- [15] Hanjae Kim, Jiyoung Lee, Seongheon Park, and Kwanghoon Sohn. Hierarchical visual primitive experts for compositional zero-shot learning. In *Proceedings of the IEEE/CVF International Conference on Computer Vision*, pages 5675–5685, 2023. 2
- [16] Xiangyu Li, Xu Yang, Kun Wei, Cheng Deng, and Muli Yang. Siamese contrastive embedding network for compositional zero-shot learning. In *Proceedings of the IEEE/CVF conference on computer vision and pattern recognition*, pages 9326–9335, 2022. 2
- [17] Yun Li, Zhe Liu, Hang Chen, and Lina Yao. Context-based and diversity-driven specificity in compositional zero-shot learning. In *Proceedings of the IEEE/CVF Conference on Computer Vision and Pattern Recognition*, pages 17037–17046, 2024. 2, 4, 6, 7
- [18] Yong-Lu Li, Yue Xu, Xiaohan Mao, and Cewu Lu. Symmetry and group in attribute-object compositions. In *Proceedings of the IEEE/CVF conference on computer vision and pattern recognition*, pages 11316–11325, 2020. 2
- [19] Victor Weixin Liang, Yuhui Zhang, Yongchan Kwon, Serena Yeung, and James Y Zou. Mind the gap: Understanding the modality gap in multi-modal contrastive representation learning. *Advances in Neural Information Processing Systems*, 35:17612–17625, 2022. 2
- [20] Yang Liu, Xinlong Wang, Muzhi Zhu, Yue Cao, Tiejun Huang, and Chunhua Shen. Masked channel modeling for bootstrapping visual pre-training. *International Journal of Computer Vision*, pages 1–21, 2024. 1
- [21] Xiaocheng Lu, Song Guo, Ziming Liu, and Jingcai Guo. Decomposed soft prompt guided fusion enhancing for compositional zero-shot learning. In *Proceedings of the IEEE/CVF Conference on Computer Vision and Pattern Recognition*, pages 23560–23569, 2023. 1, 2, 7
- [22] Xiaocheng Lu, Ziming Liu, Song Guo, Jingcai Guo, Fushuo Huo, Sikai Bai, and Tao Han. Drpt: Disentangled and recurrent prompt tuning for compositional zero-shot learning. *arXiv preprint arXiv:2305.01239*, 2023. 1, 2
- [23] Massimiliano Mancini, Muhammad Ferjad Naeem, Yongqin Xian, and Zeynep Akata. Open world compositional zero-shot learning. In *Proceedings of the IEEE/CVF conference on computer vision and pattern recognition*, pages 5222–5230, 2021. 3
- [24] Massimiliano Mancini, Muhammad Ferjad Naeem, Yongqin Xian, and Zeynep Akata. Learning graph embeddings for open world compositional zero-shot learning. *IEEE Transactions on pattern analysis and machine intelligence*, 46(3): 1545–1560, 2022. 2
- [25] Ishan Misra, Abhinav Gupta, and Martial Hebert. From red wine to red tomato: Composition with context. In *Proceedings of the IEEE Conference on Computer Vision and Pattern Recognition*, pages 1792–1801, 2017. 1, 2

- [26] Muhammad Ferjad Naeem, Yongqin Xian, Federico Tombari, and Zeynep Akata. Learning graph embeddings for compositional zero-shot learning. In *Proceedings of the IEEE/CVF Conference on Computer Vision and Pattern Recognition*, pages 953–962, 2021. 6
- [27] Muhammad Ferjad Naeem, Yongqin Xian, Federico Tombari, and Zeynep Akata. Learning graph embeddings for compositional zero-shot learning. In *Proceedings of the IEEE/CVF Conference on Computer Vision and Pattern Recognition*, pages 953–962, 2021. 2, 6
- [28] Tushar Nagarajan and Kristen Grauman. Attributes as operators: factorizing unseen attribute-object compositions. In *Proceedings of the European Conference on Computer Vision (ECCV)*, pages 169–185, 2018. 2
- [29] Peilin Yu Nihal V. Nayak and Stephen H. Bach. Learning to compose soft prompts for compositional zero-shot learning. In *Proceedings of the International Conference on Learning Representations*, 2023. 1, 2, 3, 6, 7
- [30] Senthil Purushwalkam, Maximilian Nickel, Abhinav Gupta, and Marc’Aurelio Ranzato. Task-driven modular networks for zero-shot compositional learning. In *Proceedings of the IEEE/CVF International Conference on Computer Vision*, pages 3593–3602, 2019. 1
- [31] Senthil Purushwalkam, Maximilian Nickel, Abhinav Gupta, and Marc’Aurelio Ranzato. Task-driven modular networks for zero-shot compositional learning. In *Proceedings of the IEEE/CVF International Conference on Computer Vision*, pages 3593–3602, 2019. 2
- [32] Qi Qian, Yuanhong Xu, and Juhua Hu. Intra-modal proxy learning for zero-shot visual categorization with clip. *Advances in Neural Information Processing Systems*, 36, 2024. 5
- [33] Alec Radford, Jeffrey Wu, Rewon Child, David Luan, Dario Amodei, Ilya Sutskever, et al. Language models are unsupervised multitask learners. *OpenAI blog*, 1(8):9, 2019. 5
- [34] Alec Radford, Jong Wook Kim, Chris Hallacy, Aditya Ramesh, Gabriel Goh, Sandhini Agarwal, Girish Sastry, Amanda Askell, Pamela Mishkin, Jack Clark, et al. Learning transferable visual models from natural language supervision. In *International conference on machine learning*, pages 8748–8763, 2021. 1, 3, 5, 6, 7
- [35] Frank Ruis, Gertjan Burghouts, and Doina Bucur. Independent prototype propagation for zero-shot compositionality. *Advances in Neural Information Processing Systems*, 34: 10641–10653, 2021. 2
- [36] Nirat Saini, Khoi Pham, and Abhinav Shrivastava. Disentangling visual embeddings for attributes and objects. In *Proceedings of the IEEE/CVF Conference on Computer Vision and Pattern Recognition*, pages 13658–13667, 2022. 2
- [37] Jake Snell, Kevin Swersky, and Richard Zemel. Prototypical networks for few-shot learning. *Advances in neural information processing systems*, 30, 2017. 2, 5
- [38] Qingsheng Wang, Lingqiao Liu, Chenchen Jing, Hao Chen, Guoqiang Liang, Peng Wang, and Chunhua Shen. Learning conditional attributes for compositional zero-shot learning. In *Proceedings of the IEEE/CVF Conference on Computer Vision and Pattern Recognition*, pages 11197–11206, 2023. 2
- [39] Zengyi Wo, Minglai Shao, Wenjun Wang, Xuan Guo, and Lu Lin. Graph contrastive learning via interventional view generation. In *Proceedings of the ACM on Web Conference 2024*, pages 1024–1034, 2024. 2
- [40] Guangyue Xu, Parisa Kordjamshidi, and Joyce Chai. Prompting large pre-trained vision-language models for compositional concept learning. *arXiv preprint arXiv:2211.05077*, 2022. 1, 2, 3
- [41] Guangyue Xu, Joyce Chai, and Parisa Kordjamshidi. Gipcol: Graph-injected soft prompting for compositional zero-shot learning. In *Proceedings of the IEEE/CVF Winter Conference on Applications of Computer Vision*, pages 5774–5783, 2024. 1, 2
- [42] Aron Yu and Kristen Grauman. Fine-grained visual comparisons with local learning. In *Proceedings of the IEEE conference on computer vision and pattern recognition*, pages 192–199, 2014. 6
- [43] Hongguang Zhang, Piotr Koniusz, Songlei Jian, Hongdong Li, and Philip HS Torr. Rethinking class relations: Absolute-relative supervised and unsupervised few-shot learning. In *Proceedings of the IEEE/CVF conference on computer vision and pattern recognition*, pages 9432–9441, 2021. 2
- [44] Kaiyang Zhou, Jingkang Yang, Chen Change Loy, and Ziwei Liu. Learning to prompt for vision-language models. *International Journal of Computer Vision*, pages 2337–2348, 2022. 7